Materials Science & Engineering A 755 (2019) 220–230

Contents lists available at ScienceDirect

Materials Science & Engineering A

journal homepage: www.elsevier.com/locate/msea

CAFE based multi-scale modelling of ductile-to-brittle transition of steel with a temperature dependent effective surface energy

Yang Li[a], Anton Shterenlikht[b], Xiaobo Ren[c], Jianying He[a], Zhiliang Zhang[a,*]

[a] NTNU Nanomechanical Lab, Department of Structural Engineering, Norwegian University of Science and Technology (NTNU), Richard Brikelands vei 1A, N-7491, Trondheim, Norway

[b] Department of Mechanical Engineering, University of Bristol, University Walk, Bristol, United Kingdom

[c] SINTEF Industry, Richard Brikelands vei 2B, N-7465, Trondheim, Norway

ARTICLE INFO

Keywords:
Cellular atoumata finite element (CAFE)
Ductile-to-brittle transition (DBT)
Cleavage
Effective surface energy
TMCR steel

ABSTRACT

It is still a challenge to numerically achieve the interactive competition between ductile damage and brittle fracture in ductile-to-brittle transition (DBT) region. In addition, since two types of fracture occur at two independent material length scales, it is difficult to process them with the same mesh size by using finite element method. In this study, a framework of modelling DBT of a thermal mechanical controlled-rolling (TMCR) steel is explored by using the cellular automata finite element (CAFE) method. The statistical feature of material's microstructure is incorporated in the modelling. It is found that DBT curve cannot be reproduced with only one temperature dependent flow property, for which another temperature dependent variable must be considered. A temperature dependent effective surface energy based on typical cleavage fracture stage is proposed and obtained through a continuum approach in present work. The DBT of TMCR steel is simulated by using CAFE method implemented with a temperature dependent effective surface energy. It is found that numerical simulation is able to produce a full transition curve, especially with scattered absorbed energies in the transition region represented. It is also observed that simulation results can reproduce a comparable DBT curve contrasting to the experimental results.

1. Introduction

Ductile-to-brittle transition (DBT) is normally found in the BCC materials, e.g., steel, due to temperature decreasing and loading rate elevation. Ductile fracture usually occurs at higher temperature, e.g. the upper-shelf, with a damage mechanism of void nucleation, growth and coalescence. The well-known Gurson type of model [1–4] and Rousselier model [5] have been widely used to describe ductile fracture accompanying with plastic deformation, in which the critical void volume fraction f_c has been proposed as the failure criterion. While, unstable cleavage fracture is commonly initiated by second-phase particle cracking due to dislocation pile-up, which refers to the sequence of three steps: particle breakage, transgranular fracture within a single grain and overcoming of the grain boundary [6]. A simple model proposed by Ritchie, Knott and Rice [7], so called RKR model, assumes that cleavage failure occurs when the maximum principle stress ahead of the crack tip exceeds the fracture stress σ_f over a characteristic distance. In order to describe the statistical nature of micro-cracks in the stress field, micromechanical models [8–10] following the weakest link philosophy have been reformulated based on RKR model, which provide a promising local approach to understand the essentials of cleavage. One of the most widely used approaches is Beremin model [8], in which a simple expression for macroscopic failure probability can be derived involving a scalar measure of the crack-front loading, the so-called Weibull stress σ_w. Consequently, two main types of the failure criterion for cleavage have been established, critical fracture stress σ_f or Weibull stress σ_w. Whereas, in the DBT regime, two fracture modes coexist, and the final rupture of materials occurs as a consequence of the competition between two failure mechanisms.

Modelling of DBT of steel has aroused great interest in past decades. Ductile damage models (e.g., GTN, Rousselier) combined with RKR criterion model or local approach (e.g. Beremen model) has been widely applied to model the DBT of steel under quasi-static load [11,12] or dynamic load [13–18]. However, it is basically a post-processing solution to evaluate the occurrence of cleavage after stress field ahead of crack tip obtained from the constitutive equation of ductile model. The competition between two failure mechanisms and the interaction between two failure modes in the transition region are not

* Corresponding author.
E-mail address: zhiliang.zhang@ntnu.no (Z. Zhang).

https://doi.org/10.1016/j.msea.2019.04.012
Received 4 January 2019; Received in revised form 1 April 2019; Accepted 3 April 2019
Available online 05 April 2019

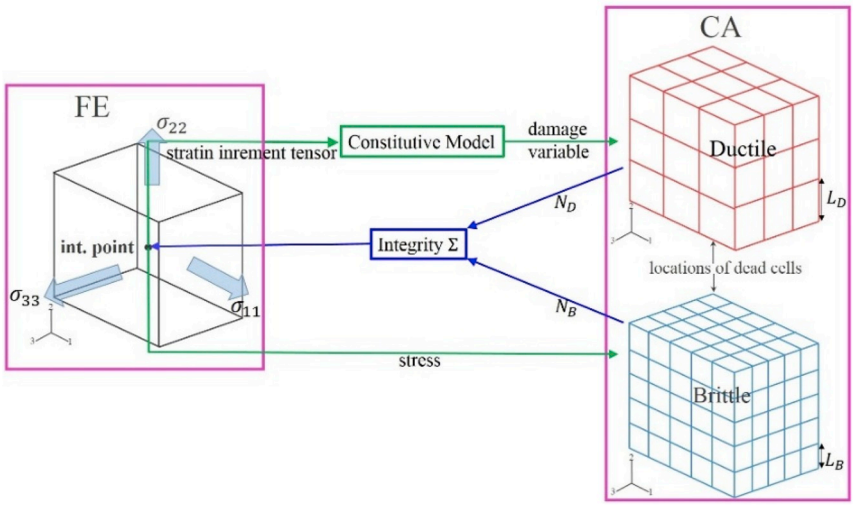

Fig. 1. The illustration of the mechanism of CAFE method in which ductile damage and cleavage fracture have been coupled through two different CA arrays. Here, N_D and N_B are the number of 'dead' cell of ductile CA arrays and brittle CA arrays respectively; Σ is integration indicator; L_D and L_B are the size of cells in brittle and ductile CA arrays.

involved indeed. Furthermore, the fracture in the transition region occurs on two independent scales of microstructure size, ductile fracture related to the spacing of the dominant void initiated from particles, while the brittle fracture related to the grain or cleavage facet size. It is difficult to handle two fracture modes with only one mesh size using the finite element method. Although attempts have been conducted to overcome this problem by using non-local approaches [11,12,19], it is still a challenge to represent the competition between two failure mechanisms and the interaction between two failure modes in the transition region. However, one approach coupled cellular automata (CA) and finite element (FE), so-called CAFE method, provides a practical solution to solve these two challenges simultaneously [20]. In addition, the statistical feature of microstructure of material can also be represented in this method, e.g. initial void distribution, grain size distribution, misoriention of grain boundaries etc., such that the scatter of toughness in the transition region can be captured. The principle and implementation of CAFE method have been thoroughly described in the ref. [20–25].

It is known that the flow properties, e.g., yield stress and strain hardening, will be altered as temperature decreases, which could be a significant factor resulting in the occurrence of DBT. However, only temperature-dependent flow stress is not enough to predict the transition behavior of materials when comparing with the test data reported by Rossoll et al. [16], Tanguy et al. [18] and Shterenlikht et al. [20]. Many efforts have been made to describe temperature dependence of fracture toughness in the DBT transition region. A global approach, Master curve method has been adopted in ASTM E1921 [26], in which the variation of fracture toughness with temperature in DBT region can be described with a reference temperature T_0. Although the Master curve method is very convenient to apply in practice since only few tests are needed for calibration, it requires high constraint and small scale yielding conditions. Tanguy et al. [18] has simulated the DBT of A508 steel with a temperature-dependent σ_u rather than a constant value when modelling the Charpy impact test. By using Master curve method [26] to calibrate the parameters of Beremin model, Petti et al. [27], Wasiluk et al. [28], Cao et al. [29] and Qian et al. [30] have also found that σ_u is increasing with temperature in the transition region. Gao et al. [31] has found that σ_u increased with temperature reflecting the combined effects of temperature on material flow properties and toughness. Moattari et al. [32] accurately predicted the fracture toughness in DBT transition region by introducing a temperature-dependent σ_u described with a summation of athermal and thermally activated stress contribution. A temperature dependent misorientation of grain boundary proposed by Shterenlikht et al. [20] has been implemented into the CAFE method to model the DBT of Charpy test of TMCR steel. It has to be noticed that either the temperature dependent σ_u or misorientation proposed in the literature is just a phenomenological parameter for DBT modelling. Therefore, exploring a physical-based variable to disclose the nature of temperature dependent fracture toughness in the transition region is not only significant but also necessary. In this work, on the basis of our previous work [33], a continuum approach is developed to estimate the effective surface energy in the DBT transition region of a TMCR steel. Then, we attempt to establish a framework of numerical prediction of the DBT in steel by utilizing the CAFE method implemented with the temperature dependent effective surface energy.

The present paper is organized as the followings. Section 2 reviews the CAFE method and discusses the parameters of the model. Section 3 introduces a continuum solution to determine the temperature dependent effective surface energy of TMCR steel. Section 4 describes the finite element procedures and models used to predict the DBT of steels. Section 5 presents the main modelling results of DBT of Charpy tests by using CAFE method implemented with a temperature dependent effective surface energy. The physical nature of the competition between particle size dominated and grain size dominated cleavage propagation is also discussed. The feasibility of CAFE method implemented with temperature dependent effective surface energy is validated by comparing the predicted results to experimental results in the literature [20]. Section 6 ends the paper with a short summary and conclusions.

2. The CAFE method

The motivation of the CAFE method is to combine the structural and microstructural interactions by finite element method [20–22]. The method is divided into two phases: one is finite elements to capture the stresses or strains at the structural level, the other is to catch the mechanical essentials of the microstructural behavior and its development in a set of CA arrays. Fig. 1 shows the implementation of the above strategy to deal with the fracture in the transition region where both ductile and brittle micro-mechanisms work simultaneously [20]. In each material integration point, the microstructure is represented by two CA arrays, where the brittle array represents the cleavage behavior while the ductile array processes ductile damage. Structural information, for example, stress/strain and damage variable, processed in FE level inputs to CA levels, meanwhile, the microstructural evolution and the failure are integrated and send back to the FEs. To achieve the

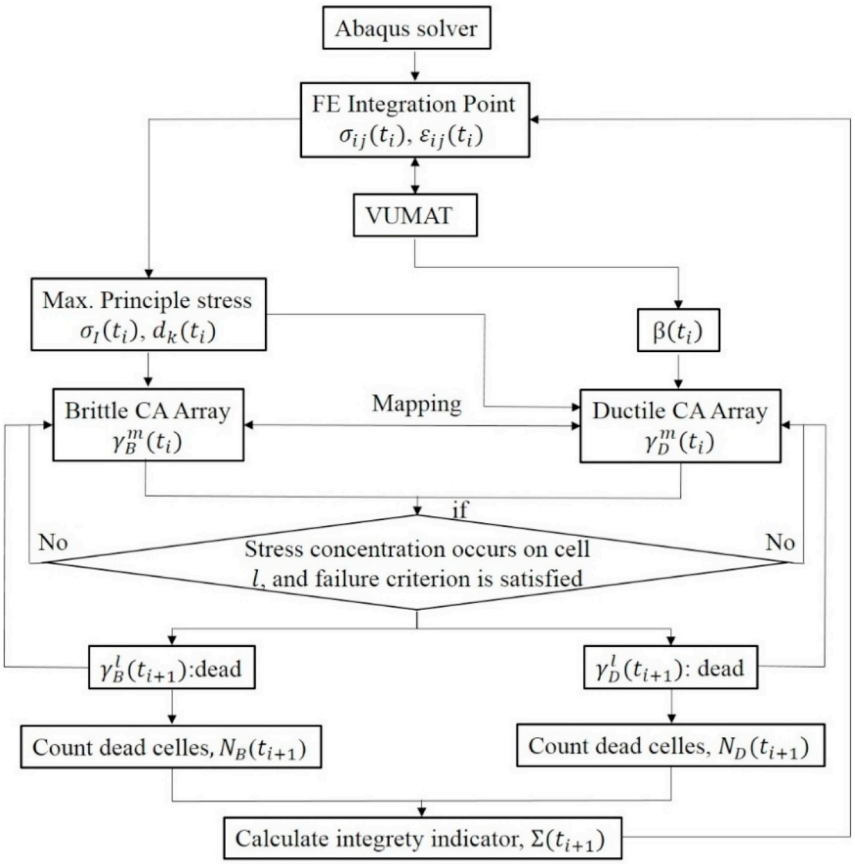

Fig. 2. Flow chart of the CAFE method. Here, $\sigma_{ij}(t_i)$ and $\varepsilon_{ij}(t_i)$ are stress and strain tensors at time t_i provided by Abaqus solver; and $\beta(t_i)$ is damage variable of cells given by constitutive model to ductile CA array at time t_i; $\sigma_I(t_i)$ is the maximum principle stress of each element calculated from $\sigma_{ij}(t_i)$; $d_k(t_i)$ is the direction cosines of $\sigma_I(t_i)$; $\gamma_D^m(t_i)$ or $\gamma_B^m(t_i)$ is state of cell m in ductile or brittle CA arrays t_i; $\gamma_D^l(t_{i+1})$ or $\gamma_B^l(t_{i+1})$ is state of cell l where stress concentration occurs and failure criterion is satisfied in ductile or brittle cell arrays at time t_{i+1}; $N_D(t_{i+1})$ or $N_B(t_{i+1})$ is numbers of dead cells in ductile or brittle CA arrays at time t_{i+1}; $\Sigma(t_{i+1})$ is the integrity indicator at time at time t_{i+1}.

implementation of CAFE method in finite element, the explicit dynamic process has been chosen to develop a VUMAT by Shterenlikht et al. [20–22] so that crack can propagate along a natural failure path through element removal.

The Roussellier ductile damage model [5] is adopted to describe the constitutive response at the integration point. Equation (1) describes the plastic potential of this model

$$\frac{\sigma_{eq}}{\rho} - H(\varepsilon_{eq}) + B(\beta)Dexp\left(\frac{\sigma_m}{\rho\sigma_1}\right) = 0 \tag{1}$$

where$H(\varepsilon_{eq})$ is the hardening property of material; σ_1 and D are material constants that need to be tuned; σ_{eq}, σ_m and ε_{eq} are equivalent stress, mean stress and equivalent strain; $B(\beta)$is the function of damage variable β; ρ is relative density, which can be described by

$$\rho = \frac{1}{1 - f_0 + f_0 exp\beta} \tag{2}$$

where f_0 is initial void volume fraction. In ductile CA arrays, cell size L_D is used to characterize the unit cell size of ductile damage of material with a single void, which normally relates to the spacing of inclusions or large carbides in steel.

According to modified Griffith theory, the critical fracture stress for cleavage can be calculated by

$$\sigma_F = \sqrt{\frac{\pi E \gamma_{eff}}{(1-\nu^2)d}} \tag{3}$$

where γ_{eff} is effective surface energy for the cleavage fracture; E and ν are Young's modulus and Poisson's ratio respectively; d is grain size. In present work, a temperature dependent effective surface energy for cleavage will be applied in the CAFE method to calculate critical fracture stress of cleavage. A fraction of brittle cells, η, in each brittle CA array, is adopted to represent grains with adjacent grain boundary carbides, where micro-crack has already nucleated. In brittle CA arrays, the cleavage facet size (d_{CFS}) is applied as the size of cells in brittle CA arrays, e.g. L_B, which can be measured through fractographic analysis on the fracture surface of specimen [20]. Since the misorientation between grains is naturally the barrier of cleavage crack propagation crossing the grain boundary [34], a random orientation is assigned to each cell in brittle CA arrays, and a misorientation threshold, e.g., θ_{th}, is assumed so that crack can propagate from one cell to the other.

The property of CA depends on the state of cells. The state of each cell in next time increment is determined by its state and the states of neighboring cells at the previous time increment. Once that the cell is failed due to the fracture propagation, the state of cell will be changed from ‘alive’, e.g., initial state, to ‘dead’. Then, the closing neighborhood of ‘dead’ cell will be stress-concentrated since the ‘dead’ cell lost its load-bearing capacity. A framework [22,25] has described in detail how to locate such a closing neighborhood around the ‘dead’ cell. The local concentration factors are utilized to solve this problem, which are C_D for ductile CA array and C_B for brittle CA array. Thus, at the next time increment, the states of concentrated cells (either ductile or brittle) are determined by the results of comparison between the product of damage variable and concentration factors and failure criteria mentioned above. An integrity indicator, Σ, is used to count the ‘dead’ cells of both ductile and brittle CA arrays by which the potential fracture at every

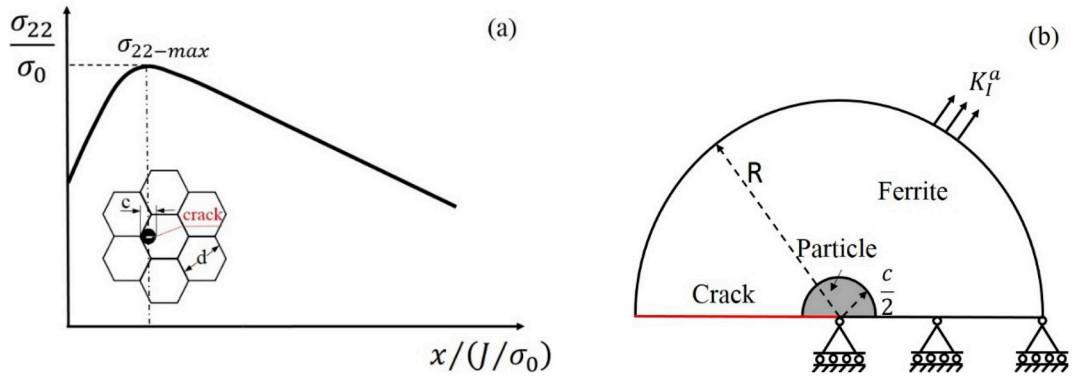

Fig. 3. The continuum model: (a) the schematic illustration of the micro-crack initiation and propagation across the interface and grain boundary, c is the particle diameter, and d is grain size; (b) MBL model to calculate the effective surface energy for cleavage extension across the interface between particle and matrix [33]. c is particle size.

current time increment is evaluated. The Σ whose initial value is 1.0, decreases continuously with the accumulation of damage until N_D or N_B reaches its maximum value N_{D-max} or N_{B-max}. At this moment, the Σ turns to be zero, which means material inside the integration point is failed and the integration point does not have loading-bearing capacity any more. The FE will then be removed from the mesh when the zero Σ is transferred to FE. The Σ can be calculated by

$$\Sigma = 1 - \max\left(\frac{N_D}{N_{D-max}}, \frac{N_B}{N_{B-max}}\right) \tag{4}$$

The calculation process of the CAFE method is presented in Fig. 2. It has to be mentioned that in order to reduce the calculation time, the damage variable $\beta(t_i)$ is given to the ductile CA array instead of the strain increment tensor $\Delta\varepsilon_{ij}(t_i)$, and accordingly only the solution dependent variable Σ is returned to the FE from CA array. Both ductile and brittle CA arrays are used only for the simulation of fracture propagation at each CA scale, while, the constitutive response is calculated at FE level. In addition, for the easy achievement of convergence, in ductile CA array a normal distribution of damage value β_F rather than that of f_0 is adopted. At each increment of deformation, the model compares the present damage variable β with the failure value β_F until the material failed. Since two CA arrays occupy the same physical space, the evaluation of the cells shall be synchronized in both CA arrays. Thus, a mapping rule has been introduced in the CAFE method to reflect dead cells in ductile CA array into the corresponding brittle CA array, and vice versa [21]. After stress concentration occurred on the cell m in either CA arrays, it becomes dead when failure criteria are satisfied. A more detailed description about the CAFE method can be found in literature [21].

3. The temperature dependent effective surface energy

Based on the theory of shielding effect of dislocation mobility on crack tip, a method has been proposed [33] to predict the temperature dependent effective surface energy of single-crystal iron in the ductile-to-brittle transition (DBT) region. In the present work, this method will be extended to calculate the effective surface energy of steel in the transition region.

The shielding effect of the dynamics of dislocation on crack tip stress field can be assessed with a continuum method [33,35,36]. It is assumed that the material is isotropic, and that the rate-dependent plastic deformation is induced by dislocation emission and motion. According to Orowan law, the shear strain rate $\dot{\gamma}^p$, can be used to describe the plasticity caused by the dislocation mobility

$$\dot{\gamma}^p = \alpha\rho_d b v \tag{5}$$

Where α is a proportionality constant; ρ_d is the dislocation density; b is Burgers vector; v is dislocation velocity. The dislocation velocity v can be obtained from the function of resolved shear stress τ and temperature Θ, e.g., the empirical Arrhenius type law

$$v = v_0 exp\left(-\frac{Q}{k_B\Theta}\right)\left(\frac{\tau}{\tau_0}\right)^m \tag{6}$$

where Q is the activation energy for dislocation velocity; k_B is the Boltzmann constant; m is a material constant for wide range of stress level; v_0 is material specific reference dislocation velocity; τ_0 is normalization shear stress; here Θ is the absolute temperature in Kelvin. Since the material is assumed to be isotropic, the von Mises equivalent stress σ_{Mis} and the equivalent plastic strain rate $\dot{\varepsilon}^p$ can be used to replace the plastic shear strain rate $\dot{\gamma}^p$ in equation (5) and the resolved shear stress τ in equation (6). Then, after inserting the equation (6) into equation (5), the equivalent plastic strain rate $\dot{\varepsilon}$ to describe the rate-dependent plasticity induced by the dislocation mobility can be derived

$$\dot{\varepsilon} = \dot{\varepsilon}_0 \exp\left(-\frac{Q}{k_B\Theta}\right)\left(\frac{\sigma_{Mis}}{\sigma_0}\right)^m \tag{7}$$

where $\dot{\varepsilon}_0$ is a reference strain rate; σ_0 is a normalization stress.

It is known that DBT normally occurs in body centered cubic (BCC) metals, e.g., single-crystal iron, Fe alloys and steel, due to the thermal-activated dislocation emission and motion [37]. The difference between single-crystal iron and steel is the presence of impurities (e.g., particles), grain boundary and preexisting dislocations in the latter, which affects the dislocation behavior, for instance, nucleation, motion, multiplication etc. If their effect on the fracture of the latter can be described by the change of dislocation density near crack tip comparing with that of former, see equation (5), the model developed for single-crystal iron is possible to be applied to the steel according to the theory of the of shielding effect of dislocation mobility on crack tip. To do this, several assumptions have to be made. Firstly, a micro-crack is assumed to be initiated within a grain boundary particle, e.g., carbide or inclusion, at a position x_c ahead of the notch/crack tip where the local tensile stress equals to the maximum principle stress, see Fig. 3 (a). Then, the nucleated micro-crack will penetrate the interface between particle and matrix once that local tensile stress at the interface exceeds the fracture stress. Secondly, we postulate that the penetration of the micro-crack into the interface leads to the final unstable cleavage fracture, namely the crack resistance of grain boundary is not taken into account. Further, it is assumed that the crack penetration from particle into matrix is dominated by a local K-field. Then, the elastic zone (dislocation free zone) in the continuum model for single-crystal material [33] is replaced with an elastic particle, and the viscoplasitic material outside the elastic region is defined as the ferrite, e.g., a time-dependent plastic matrix. Thus, a new continuum model can be adopted to estimate the fracture toughness of steel in the transition region, see

Fig. 3 (b).

Only the upper-half of model is presented due to symmetry, see Fig. 3 (b). A small circle around the crack tip with a radius $c/2$ is the elastic zone, e.g., particle. The radius of model R is 20 times larger than the elastic zone size. Outside the elastic zone, there is the matrix, e.g., ferrite, which is time-dependent plastic material described by the equation (7). A crack with an initial radius of $1.15 \times 10^{-4}R$ is located in the center of model. Abaqus 6.14 is employed, and 4-node and plane strain elements (CPE4) are used in all simulations. Through the nodal displacement on the outer boundary layer in the MBL model, a linear elastic K_I field, e.g., the applied stress intensity factor K_I^a, with a constant loading rate $\dot{K}$ is implemented. To calculate the effective surface energy, only a stationary crack is studied.

For a sharp crack tip, cleavage fracture occurs once the crack tip stress intensity factor equals to the critical value, i.e.$K_I^t = K_{IC}$. The critical stress intensity factor K_{IC} depends only on the material's surface energy γ_s in terms of the Griffith criterion. Due to the shielding effect of plastic deformation on the crack tip stress field, the local stress intensity factor K_I^t at crack tip is always lower than the applied stress intensity factor K_I^a, particularly at higher temperature. The applied stress intensity factor K_I^a at the moment of failure, e.g. $K_I^t = K_{IC}$ is regarded as the fracture toughness of material. According to modified Griffith theory$G_c = 2(\gamma_s + \gamma_p)$, if let $\gamma_s + \gamma_p = \gamma_{eff}$, the effective surface energy can be obtained by

$$\gamma_{eff} = \frac{(1-\nu^2)}{2E}K^2 \tag{8}$$

Thus, the applied stress intensity factor K_I^a at cleavage fracture can be calculated, and accordingly the effective surface energy for cleavage extension across the particle-matrix interface of steel in the transition region can also be obtained from equation (8).

4. Numerical simulation

An explicit dynamic process is adopted to model the Charpy test by using an explicit code with CAFE strategy implemented, which has been introduced in Section 2. The geometry of Charpy V-notch specimen is 55 mm*10 mm*10 mm according to the standard ASTM E23 16b [38], the notch radius and notch depth are 0.25 mm and 2.0 mm respectively. The striker and anvils size and geometry are also those of the standard ASTM E23 16b [38]. The finite element model of Charpy test is shown in Fig. 4, in which the full Charpy specimen is meshed with 8 nodes and reduced integration elements (C3D8R). Cells are assembled only to those elements in a small region in the center of specimen with a mesh size around 1 mm, so-called damage zone, where damages in a real Charpy specimen is expected. The striker and two anvils are modelled as elastic body, and are meshed with C3D8R and C3D6 type of elements. The total number of elements in this model is 8250, in which damage zone composes of 700 elements. The contact between the Charpy specimen and striker and anvils is modeled with a friction coefficient 0.15. The initial velocity of striker is 5.5 m/s.

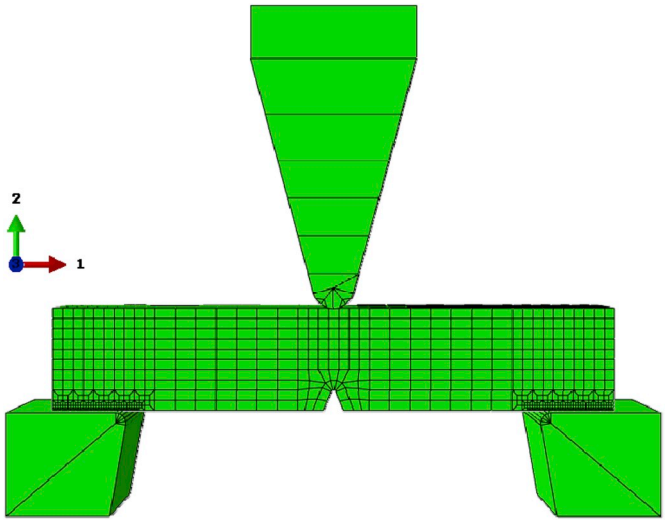

Fig. 4. Finite element model of the Charpy test.

It is assumed that L_D and L_B are $200\mu m$ and $100\mu m$ respectively. Then, in the ductile CA arrays, each cubic array has 5 cells per linear dimension, namely $m_D = 5$. Likewise, in the brittle CA arrays, each cubic has 10 cells per linear dimension, namely $m_B = 10$. Therefore, in each element or integration point, there are 125 ductile cells and 1000 brittle cells. Accordingly, the damage zone is composed of 87500 ductile cells and 700000 brittle cells. It is assumed that the CA array either ductile or brittle loses the load-bearing capacity when the cells in one orthogonal section of CA array are failed [21]. Therefore, the maximum numbers of the dead cells in each CA array are taken as $N_{D-max} = m_D^2 = 25$ for ductile CA arry and for the brittle CA array. The concentration factor for ductile CA, e.g., C_D, is 1.4 and that for brittle CA, e.g., C_B, is 1.4 and 11.0 respectively [20].

The initial void volume fraction f_0 is assumed to be 0.0001. The statistical feature of damage failure value β_F conforms to a normal distribution, in which the mean value β_{F-mean} is 8.0 and the standard deviation β_{F-std} is 1.2. The material constant D and σ_1 are 1.65 and 400 MPa respectively. These values of ductile damage variables used in the present work has been calibrated with experimental results of pure ductile fracture, for example the upper shelf energy (USE) of Charpy test. The flow property of the TMCR steel at different temperature is presented in Fig. 5 (a). The microstructure of this TMCR steel is presented in the Fig. 5 (b), which consists mainly of ferrite and some banded pearlites. Based on the measurement of grain size of this TMCR steel, the histogram of grain size distribution is obtained as shown in the Fig. 5 (c), which presents a bimodal distribution. Since these tiny grains will never fracture as they have very high fracture strength, the modelling results are not affected by omitting this small volume of tiny grains. Hence, an equivalent unimodal three-parameter Weibull distribution is applied to characterize the grain size distribution of this material, in which the scale, shape and location parameter are 1.223, 5.392 and 0.516 respectively. The fraction of brittle CA cells that cleavage is nucleated, η, is assumed to be 0.01, which has been adopted by Shterenlikht et al. [20] as well. The misorientation threshold θ_{th} is assumed to be 40°. The effective surface energy for the fracture stress of cleavage will be calculated in the section 5.

5. Numerical results and discussion

In the following, we firstly present the predicted results of DBT by using a constant effective surface energy. To reproduce the transition by using the CAFE method, another temperature dependent variable, e.g., the temperature dependent effective surface energy, is calculated via the continuum approach introduced in the Section 3. Although being improved, the DBT predicted with the calculated temperature dependent effective surface energy indicates that the role of grain boundary in the cleavage propagation in the transition region cannot be neglected. As such, the lower limit of effective surface energy for overcoming the barrier of grain boundary in the transition region is estimated based on both the temperature dependent effective surface energy for unstable cleavage formation and the size ratio of cleavage facet (unit) to critical particle. In the end, an accurate prediction of DBT of TMCR steel is achieved by using the lower limit of effective surface energy for crack propagating across the grain boundary.

5.1. DBT prediction by using a constant effective surface energy

Firstly, a constant value of the effective surface energy γ_{eff}, $52J/m^2$, which has been adopted in the study on the DBT of TMCR steel by Wu

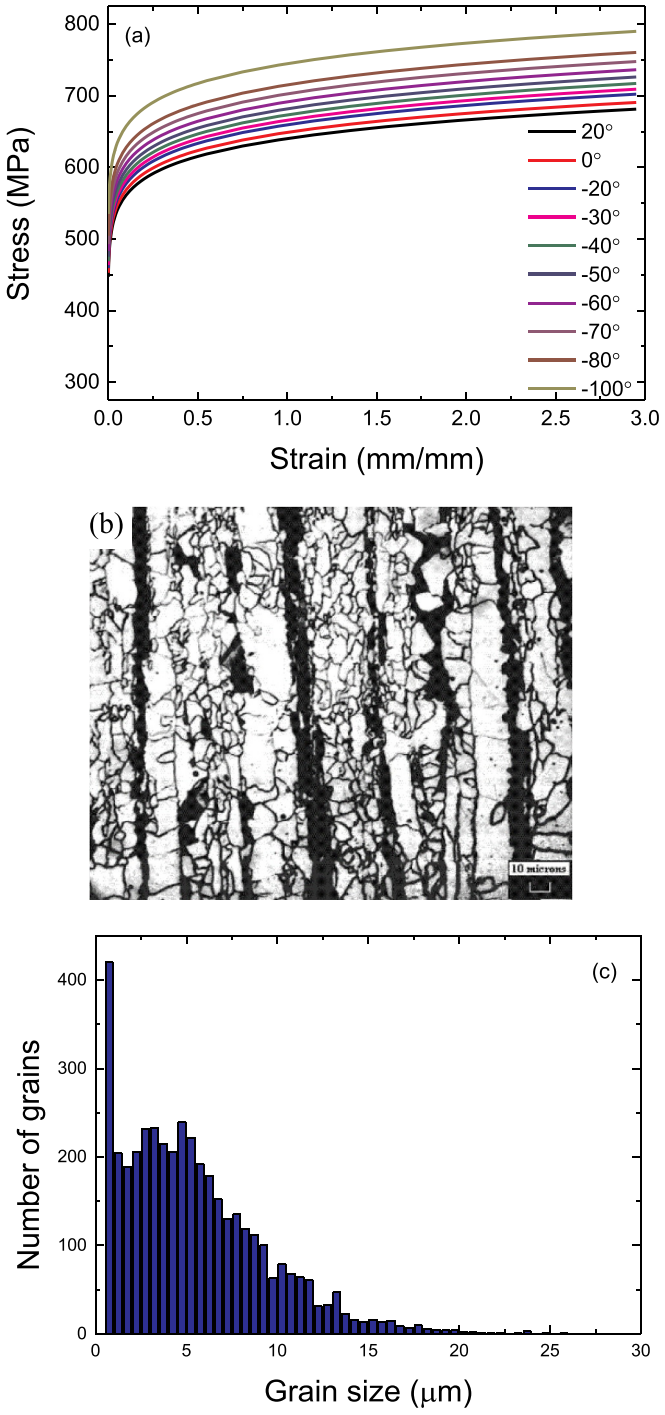

Fig. 5. The properties and microstructure of TMCR steel: (a) flow stress and strain curve at different test temperatures [21], (b) the microstructure of TMCR steel [20] and (c) the histogram of grain size distribution [20].

et al. [23] and Shterenlikht et al. [20], is used in the CAFE method to calculate the fracture stress of cleavage according to equation (3). The other parameters to model the DBT of TMCR steel have been introduced in the Section 4. The absorbed energy of standard Charpy tests in the transition region vs. temperature is plotted in the Fig. 6, in which the predicted results by CAFE method with constant effective surface energy compare with the experimental results by Shterenlikht et al. [20]. At each temperature, three runs have been performed. Since the statistical nature of material has been incorporated in the model, results present a scattered feature as shown in the Fig. 6. It can be found that

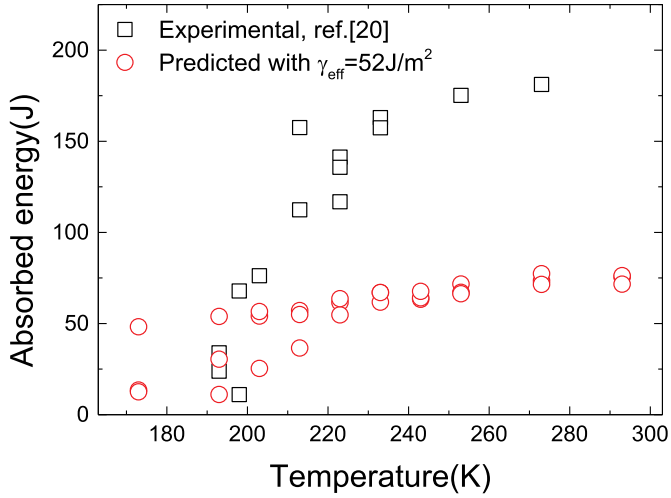

Fig. 6. Absorbed energy of Charpy impact test in the transition region predicted by CAFE model with a constant effective surface energy, e.g..$\gamma_{eff} = 52J/m^2$.

the predicted absorbed energy at higher temperature is not as scattered as that at lower temperature since the fewer cleavage happens at higher temperature. The predicted absorbed energy at lower temperature, e.g., 193 K, is comparable to the experimental results. However, the predicted absorbed energy is dramatically underestimated comparing to the experimental results. It implies that only temperature-dependent flow stress of material shown in Fig. 5 (a) is not adequate to obtain an ideal DBT behavior, which has been similarly reported by Rossoll et al. [16], Tanguy et al. [18] and Shterenlikht et al. [20]. Thus, the second temperature-dependent parameter has to be searched so as to accurately represent the DBT behavior of materials.

5.2. The effective surface energy of TMCR steel

5.2.1. Identification of the parameters

It is found that the variation of activation energy of DBT among single-crystal iron, poly-crystal iron and Fe-alloys is relatively minor [39,40], e.g., in the range of 0.2–0.5. This implies that the minor difference between parameters calibrated from the activation energies of DBT of different steels can be expected. In addition, there are still some resemblances between low carbon steel studied by Tanaka et al. [40] and the TMCR steel investigated in the present work, e.g., the ferritic type of microstructure and controlled-rolling process of production. Since the absence of the test results of activation energy of DBT of the TMCR steel, a low carbon steel experimentally obtained by Tanaka et al. [40] is utilized to approximately identify the parameters for the calculation of effective surface energy of the TMCR steel. In the aim of exploring a solution to estimate the effective surface energy in transition region, the gap between two materials, e.g., low carbon steel and the TMCR steel can be ignored.

As reported in the literature, a relation between loading rate $\dot{K}$ and Θ_c has been found through experiments [41].

$$ln\dot{K} = -E_a/k_B\Theta_c + const. \quad (9)$$

where E_a is the activation energy for the DBT, which equals to the activation energy Q for dislocation velocity; Θ_c is critical DBT temperature at which ductile fracture changes to be brittle fracture [33,35,36]. Based on the theory of shielding effect of dislocation mobility on crack tip, equation (9) has also been used to depict the correlation of loading rate and Θ_c of low carbon steel by Tanaka et al. [40]. The critical transition temperatures of low carbon steel have been measured through four point bending tests under different outer-fiber strain rates by Tanaka et al. [40]. The outer-fiber strain rate can be calculated by Ref. [42].

$$\dot{\varepsilon}_f = \frac{4B}{S_1^2}\dot{\delta} \tag{10}$$

where $\dot{\varepsilon}_f$ is the outer-fiber strain rate and $\dot{\delta}$ is the cross head speed, B is the thickness of specimen and S_1 is the outer span of specimen. The applied stress intensity factor of four point bending test can be calculated by using the equation [43].

$$K_I = \frac{3F(S_1 - S_2)}{2BW^2}\sqrt{a}\,Y \tag{11}$$

where $Y = \frac{1.1215\sqrt{\pi}}{(1-a/W)^{3/2}}\left[\frac{5}{8} - \frac{5}{12}\frac{a}{W} + \frac{1}{8}\left(\frac{a}{W}\right)^2 + 5\left(\frac{a}{W}\right)^2\left(1 - \frac{a}{W}\right)^6 + \frac{3}{8}\exp\left(-6.1342\frac{a}{W-a}\right)\right]$, F is loading force, S_2 is inner span, W is width of specimen and a is notch depth. To obtain the loading rate of four point bending test, three-dimensional analysis with a quasi-static process is carried out in the present study. The cross head speed applied for modelling is converted from outer-fiber strain rates used by Tanaka et al. [40] in terms of the equation (10). It has to be mentioned that only a stationary crack is studied. The Young's modulus $E$and poison's ratio $\nu$of steel are 206 GPa and 0.29 respectively. The loading rate, e.g., the rates of stress intensity factor, applied on the four-point bending specimen is calculated by equation (11). The outer-fiber strain rates and calculated loading rate, e.g., the applied rates of stress intensity factor are listed in Table 1.

The critical DBT temperature under a specific loading rate can be predicted by using the continuum approach introduced in section 3. Different elastic zone size (e.g., particle size) of the model is also studied. To obtain the critical DBT temperatures under the loading rates listed in Table 1, for each elastic zone size, several groups of parameters have been tried following the method introduced previously by the authors [33]. By doing this, groups of parameters are optimized for each elastic zone size, which are listed in the Table 2. The computed DBT temperatures under different loading rates are compared with experimental results by Tanaka et al. [40] in Fig. 7. It is shown that the computational results of low carbon steel agree well with experimental results, which indicates that the group of parameters for each elastic zone size is reliable. Meanwhile, the influence of the elastic zone size on the fracture toughness in the transition region is also studied under the loading rate 10 $\mathrm{MPam}^{0.5}s^{-1}$. The applied stress intensity factor K_I^a normalized with the critical stress intensity factor K_{IC} vs. temperature are plotted in the Fig. 8 for each elastic zone size. Here, $K_{IC} = 1.77MPam^{0.5}$ is calculated from the widely used effective surface energy for cleavage of steel, e.g., $7J/m^2$, tested by Bowen et al. [44] according to Griffith theory. It is shown in Fig. 8 that to achieve an identical DBT temperature Θ_c the minor difference among the fracture toughness for different elastic zone sizes is presented in the whole temperature range by using the parameters identified above. Recall the equations (5)–(7), at a specific temperature and under same stress level, when activation energy Q is determined, with the combination of parameter of $\dot{\varepsilon}_0$ and m, the similar amount of shielding effect of dislocation dynamics and DBT behavior can be always achieved no matter how large the elastic zone size (particle size) is. To this end, it can be concluded that the predicted DBT of low carbon steel by using the continuum model is elastic zone size independent. In the later simulation, the parameters verified for elastic zone size 1 μm will be adopted.

Table 1
The outer-fiber strain rates of the four point bend tests on fully annealed low carbon steel [43] and the calculated applied rates of stress intensity factor.

$\dot{\varepsilon}(s^{-1})$	$\dot{K}_I^a(\mathrm{MPam}^{0.5}s^{-1})$
4.46e-4	2.5790
2.23e-4	12.897
1.12e-2	64.774

Table 2
Parameters for different elastic zone size.

$c/2$	$\dot{\varepsilon}_0(s^{-1})$	$Q(ev)$	m	σ_0
0.25	29934.39	0.236	1.45	1.0
0.50	11307.01	0.236	1.70	1.0
1.0	3898.48	0.236	2.00	1.0
2.0	1717.67	0.236	2.30	1.0

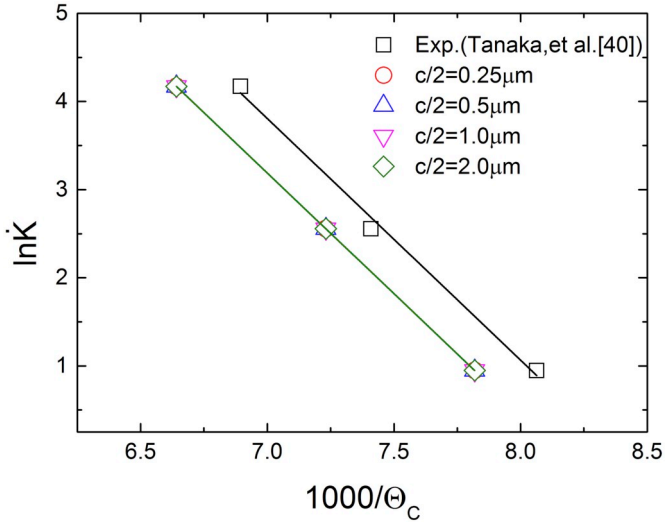

Fig. 7. Comparison of computed and experimental critical DBT temperature of low-carbon steel.

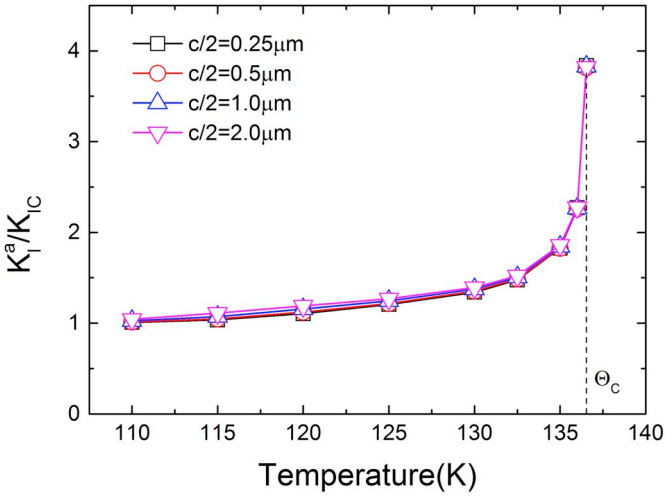

Fig. 8. The DBT curve of steel predicted by the continuum model with different elastic zone size. The loading rate is 10 $\mathrm{MPam}^{0.5}\mathrm{s}^{-1}$.

5.2.2. The temperature dependent effective surface energy

As mentioned above, the shielding effect of dislocation mobility on crack tip is loading rate dependent. To obtain the loading rate of Charpy impact test, the three-dimensional analysis of Charpy test is conducted. The geometry of Charpy V-notch specimen is identical to that introduced in the section 4. To model the transient process of impact and obtain the J-integral from Abaqus, a dynamic implicit process is utilized. However, only a stationary crack is studied here. The V-notch Charpy impact specimen is actually replaced by U-notch specimen in the calculation of J-integral since that the identical J-integrals calculated by Abaqus have been obtained from both notch-type specimen with same radius in present study. A path-independence pattern is

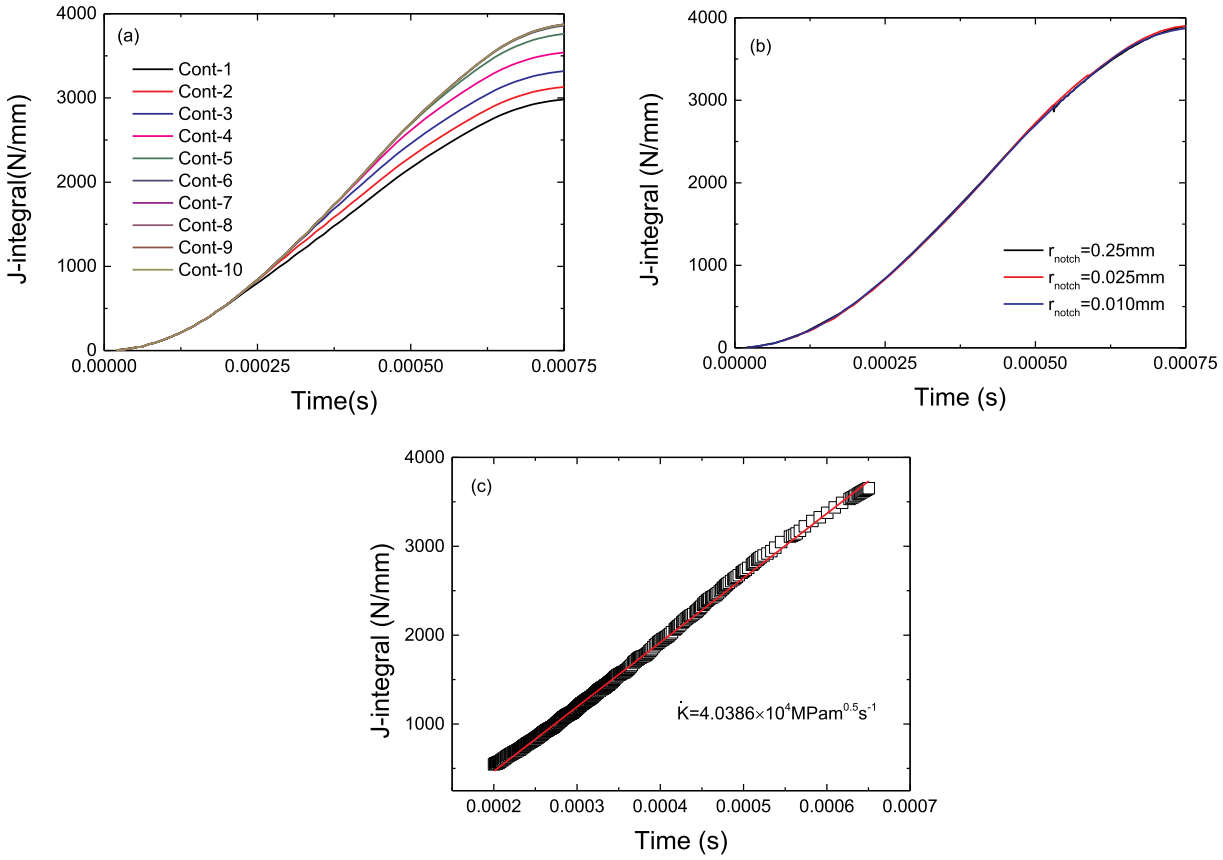

Fig. 9. Charpy impact test modelling results: (a) path-independence of J-integral of U-notch specimen with notch radius 0.25 mm, (b) J-integral of Charpy impact tests with different notch radius, (c) the loading rate of Charpy impact test. Here, r_{notch} is the notch radius of Charpy specimen.

presented in the Fig. 9 (a) in a relative far field (beyond the 5 contours) near notch root. A notch radius independence of J-integrals is presented in Fig. 9 (b). The loading rate $\dot{K}$ of Charpy impact test, $4.0386 \times 10^4 \mathrm{MPam}^{0.5}\mathrm{s}^{-1}$, is achieved by fitting the linear part of the curve of J-integral vs. time as shown in Fig. 9 (c).

By applying continuum approach shown in Section 3, the fracture toughness of the TMCR steel in the DBT region is calculated with parameters identified in section 5.2.1 and the loading rate of Charpy impact test calculated above. According to equation (8), the effective surface energy of TMCR steel in the transition region is calculated as shown in Fig. 10. It can be found that the effective surface energy of steel in the lower temperature, e.g. below 200 K, is very stable and comparatively low. However, it increase rapidly until the critical DBT temperature when temperature beyond 220 K. In addition, an equation for describing the correlation between the effective surface energy and temperature is obtained by fitting the calculated effective surface energy at different temperature, see Fig. 10. This equation for temperature dependent effective surface energy will be adopted in the later simulation of DBT of TMCR steel.

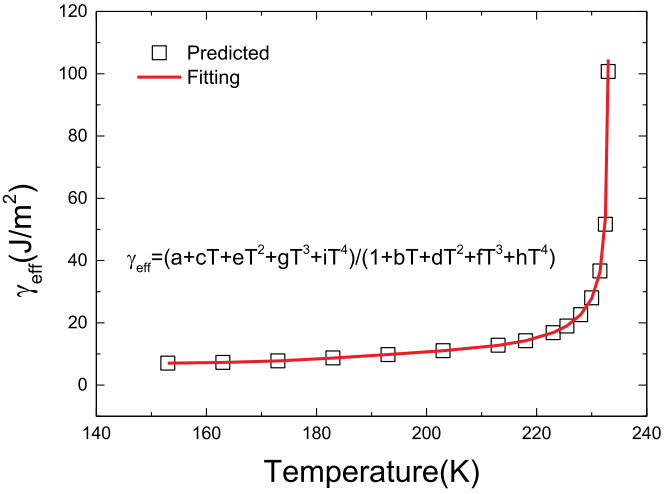

Fig. 10. The calculated effective surface energy in the transition region by using continuum model, where a, b, c, d, e, f, g, h, i are constant.

5.3. DBT of TMCR steel modeled with an effective surface energy

A temperature-dependent effective surface energy law obtained in Section 5.2 (see Fig. 10) is applied to the CAFE method to simulate the DBT of TMCR steel. Here, the procedure and parameters used for the modelling are identical to those utilized in the Section 5.1 except that a constant value of the effective surface energy is replaced by the temperature-dependent effective surface energy. The predicted absorbed Charpy energy vs. temperature is plotted in the Fig. 11, in which the experimental results are also presented for comparison. It can be observed that the DBT transition happens in a very narrow temperature range and a dramatic steep transition are obtained comparing with the experimental results. In addition, both lower shelf and upper shelf of DBT are obviously underestimated.

In the process of the unstable cleavage propagation of steel, the second step is critical in terms of the formation of unstable fracture [45], otherwise the crack stops or be blunted at the interface, and then the cracked particle may act as the nuclei for void growth when ductile fracture intervenes. The critical fracture stress for the crack propagation across the interface between the particle and matrix, e.g., particle cleavage strength σ_{pm} [46], can be calculated by

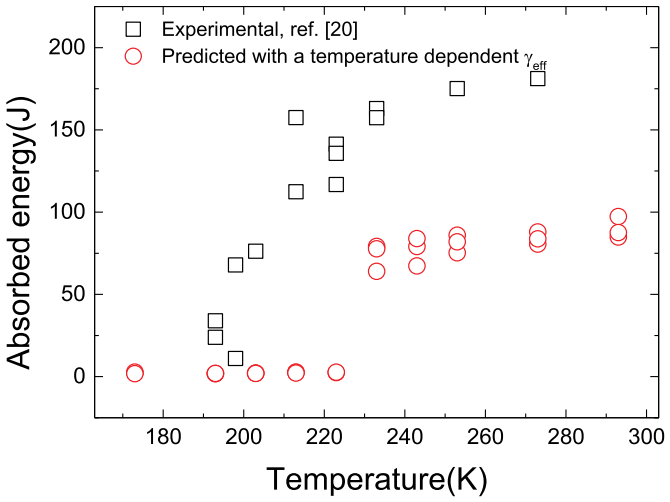

Fig. 11. Absorbed energy of Charpy impact test in the transition region predicted by CAFE method with a temperature-dependent effective surface energy.

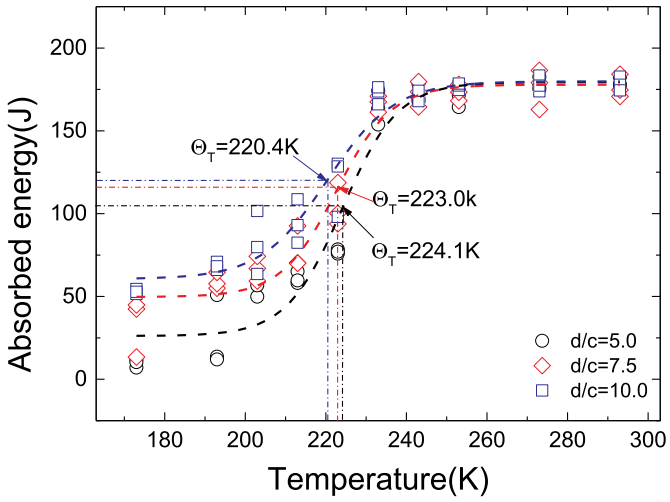

Fig. 12. The predicted DBT of TMCR steel with different ratios of d/c. Here, data is fitted by the sigmoidal method. The transition temperature Θ_T is defined as the temperature corresponding to the impact energy halfway between the lower shelf energy (LSE) and USE [49].

$$\sigma_{pm} = \left(\frac{\pi E \gamma_{pm}}{(1-\nu^2)c}\right)^{1/2} \tag{12}$$

where γ_{pm} is the effective surface energy to propagate the micro-crack across particle-matrix interface; c is the particle size. Once unstable fracture formatted, e.g., micro-crack initiation from the particle and penetration into the matrix, the first grain boundary could be the barrier for unstable cleavage crack to trespass, see Fig. 3 (a). The critical fractures stress, e.g. grain strength σ_{mm} [46], becomes a criterion for the extension of the crack across the grain boundary, which can be described as

$$\sigma_{mm} = \left(\frac{\pi E \gamma_{mm}}{(1-\nu^2)d}\right)^{1/2} \tag{13}$$

where γ_{mm} is the effective surface energy for crack propagation across the grain boundary; d is grain size. Comparing with the equation (14), it indicates that

$$\frac{\sigma_{mm}}{\sigma_{pm}} = \frac{\gamma_{mm}}{\gamma_{pm}}\frac{c}{d} \tag{14}$$

When the local stress near the particle $\sigma_L = \sigma_{mm} < \sigma_{pm}$, the micro-crack could propagate across the grain boundary, and unstable cleavage fracture would be ensured by the particle cracking. It implies that the unstable fracture is dominated by the particle size, e.g., cleavage at the lower shelf, where the local stress near the particle is high enough due to the higher yield stress. However, when $\sigma_L = \sigma_{mm} > \sigma_{pm}$, the crack arrests at the grain boundary, resulting in the appearance of stable and grain-sized micro-crack. It means that the propagation of unstable fracture is dominated by the grain size, e.g., cleavage occurring in the transition region, where the local stress near the particle is not adequate to overcome the grain strength. Therefore, it can be concluded that the role of grain boundary on the unstable cleavage propagation should not be neglected, and that the cleavage propagation in the transition region depends on the competition between σ_{mm} and σ_{pm}, e.g., particle dominated or grain size dominated [46–50].

A critical condition for crack propagating across the first grain boundary can be deduced from the equation (14) when σ_{mm} equals to σ_{pm}, from which the lower limit of the effective surface energy for crack extension across the grain boundary can be achieved

$$\gamma_{mm} = \gamma_{pm}\frac{d}{c} \tag{15}$$

It implies that the minimum of γ_{mm} is solely related the size ratio of grain and particle when the effective surface energy of cleavage formation of the material, e.g., γ_{pm}, has been obtained. As such, the γ_{pm} can be transferred to γ_{mm}, by using equation (15). Recall the equation (3), theγ_{mm} is exactly required to calculate the fracture stress of cleavage in CAFE method. While, the effective surface energy obtained in the section 5.2, it is actually not the γ_{mm} but theγ_{pm}, which is the reason why the absorbed energies in the full temperature range is underestimated as shown in the Fig. 11.

Based on the γ_{pm} obtained in Section 5.2, DBT of the TMCR steel is predicted with the variable ratio of d/c as shown in the Fig. 12. It can be observed that different ratio of d/c can achieve a similar upper shelf, while the lower shelf and the absorbed energy in transition region are quite different. Since complete ductile fracture happens on the upper shelf, the ratio of d/c presents no effect on the absorbed energy, which is usually only relevant to the cleavage fracture. It is also found that the larger ratio of d/c enables a higher absorbed energy of steel in the temperature range below the upper shelf. Meanwhile, a lower transition temperature, Θ_T, is achieved for the larger ratio of d/c. San Martin et al. [47] has studied the cleavage fracture in the transition region of Ti-V alloyed steel, in which some isolated cleavage islands could be formed surrounded by ductile fracture. They have measured the sizes of cleavage islands, e.g., d_{CL} and the sizes of cleavage initiators, e.g. $c_{crit.}$. The effective surface energyγ_{mm} has been calculated by using a similar transferring rule (e.g., equation (15)), in which the effective surface energy γ_{pm}=7 J/m^2 has been adopted. It has been found that the γ_{mm} lineally increases with the ratio of $d_{CL}/c_{crit.}$ measured at all temperatures in DBT regime. This proves that the ratio d/c in equation (15) can physically reflect the toughness of material as shown in Fig. 12.

It is well known that the particle precipitated in the steel is non-uniformly distributed for both size and spacing. Ahead of the crack/notch tip, the particle is sampled as the cleavage nucleate once the maximum principle stress ahead of the crack/notch tip is higher than σ_{pm}, see equation (12). However, the stress ahead of the crack/notch tip generally decreases with the temperature, which means that accordingly the size of qualified particle to be sampled as the initiator of cleavage decreases with the decrease of temperature. A linear relation between temperature and critical particle size has been found in SA 508 steel by Lee et al. [51]. Since the grain size is temperature independent, it implies that the ratio of d/c is not a constant value in the transition regime but a variable relevant to the temperature. In addition, the crystallographic unit of cleavage could not be the grain size, since crack deflection or arrest usually does not happens at the lower grain boundary. Whilst, it has been pointed out that the cleavage fracture unit

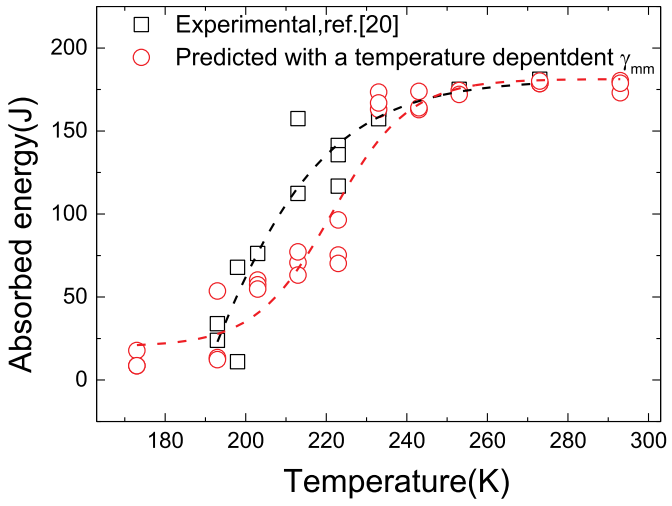

Fig. 13. Absorbed energy of Charpy impact test in the transition region predicted by CAFE method with a temperature-dependent effective surface energy corrected by a temperature dependent ratio of $d_{CF(U)S}/c_{crit.}$. Here, data is fitted by the sigmoidal method.

(facet) size or the effective grain size is more suitable to describe the cleavage fracture unit, and that both of them match each other very well in Mn-Mo-Ni low alloy steel [52]. To accurately describe the competition between σ_{pm} and σ_{mm} of cleavage fracture in the transition region, the grain size d in equation (15) should be modified to the cleavage facet (unit) size $d_{CF(U)S}$ or effective grain size d_{EGS}. According to the findings by Lee et al. [51], a linear relation between the ratio of $d_{CF(U)S}/c_{crit.}$ or $d_{EGS}/c_{crit.}$ and temperature could be expected since that the $d_{CF(U)S}$ is generally temperature independent. To this end, a linear correlation between $d_{CF(U)S}/c_{crit.}$ and temperature is assumed

$$\frac{d_{CF(U)S}}{c_{crit.}} = -0.025(\Theta - 273) + 4.0 \tag{16}$$

where Θ is temperature. Then, the effective surface energy obtained in section 5.2 as shown in Fig. 10 is corrected by the ratio of $d_{CF(U)S}/c_{crit.}$ in equation (16) according to the equation (15), from which the γ_{mm} can be obtained. Then, the calculated γ_{mm} is implemented in CAFE method to predict the DBT of TMCR steel. The predicted absorbed energy vs. temperature is plotted in the Fig. 13, in which the experimental results of TMCR steel is also presented for comparison. It is observed that simulation is able to produce a full transition curve with a scatter pattern of absorbed energies in the transition region. Generally, the predicted transition curve is comparative to the experimental results. The simulation can reproduce a similar LSE and USE comparing with the experimental results, while the absorbed energy in transition region is slightly underestimated comparing with the experimental results.

It is not surprising for the underestimation of the absorbed energy in the transition region as shown in Fig. 13 because that the γ_{mm} estimated from equation (15) is just its lower limit. Actually, it is very difficult to precisely measure or predict the effective surface energy for crack propagating across the grain boundary [47,50]. In the section 5.2, a constant exponent m that describes the correlation between dislocation velocity and resolved shear stress is used to estimate the effective surface energy of unstable cleavage formation (e.g., the second step) in the transition region, see equations (6) and (7). However, it has been found that m decreases with the increase of temperature [53,54], which means that the fracture toughness in transition region could be underestimated since the lower m can lead to a higher toughness [35] in the transition region. Accordingly, the γ_{pm} for cleavage penetration into matrix could be under-predicted as well. This could be a reason why the predicted absorbed energies in the transition region are lower than those of experimental results as shown in Fig. 13. Since the lacking of the experimental correlation between the ratio of $d_{CF(U)S}/c_{crit.}$ and temperature for this TMCR steel, an artificial linear relation between them is assumed to transfer the γ_{pm} to γ_{mm}, which is inspired by the study in Ref. [51]. Therefore, measurements on the critical particle size and the cleavage facet (unit) size of steel have to be conducted so as to find a more reliable temperature dependent ratio of $d_{CF(U)S}/c_{crit.}$.

6. Conclusions

In this study the CAFE method developed by Shterenlikht et al. [20–22] has been applied to mitigate some of the computational challenges in modelling of DBT and incorporate the statistical nature of microstructure at the same time. In order to realistically capture the temperature dependent fracture toughness in the transition region, a physical based variable has to be searched, which is also one of the motivations of this work. On the basis of our previous work [33] a continuum approach has been developed to estimate the effective surface energy for unstable cleavage formation, e.g., γ_{pm}. Further, to describe the essence of the competition between particle size and grain size controlled propagation of unstable cleavage, a more robust variable, effective surface energy for overcoming the barrier of grain boundary, e.g., γ_{mm}, was proposed. Finally, a framework for the modelling of DBT is explored through implementing the γ_{mm} into the CAFE method. Some important findings obtained in present work can be summarized as followings:

- It is proved that a second temperature dependent variable has to be found to reproduce the DBT curve, in addition to the temperature dependent flow properties. In present work, a continuum approach has been developed to establish the second temperature dependent variable, e.g., γ_{pm}.
- It is observed that the role of grain boundary on the unstable cleavage propagation cannot be ignored. Through analyzing the competition between the particle size and grain size dominated unstable cleavage propagation, a method to quantify the lower limit of γ_{mm} has been built.
- Due to the fact that cleavage facet (unit) size or effective grain size, e.g., $d_{CF(U)S}$, rather than the grain size is more appropriate for characterizing the cleavage fracture unit, the ratio of grain size to critical particle size has been replaced by $d_{CF(U)S}/c_{crit.}$ in the estimation of γ_{mm}.
- It is found that numerical simulation by using the CAFE method implemented with $\gamma_{mm}$is able to produce a full transition curve, especially with scattered absorbed energies in the transition region represented.

Although a framework of modelling DBT of steel is explored in this work, it still has some limitations. More experimental results are required for the calibration of parameters to calculate the temperature effective surface energy adopted in present work, for instance, the activation energy for the DBT and the temperature dependent ratio of $d_{CF(U)S}/c_{crit.}$ of the TMCR steel. In addition, the adiabatic heating effect and viscoplastic of material is not considered in Charpy impact modelling.

Acknowledgements

The authors wish to thank the Research Council of Norway for funding through the Petromaks 2 Programme, Contract No.228513/E30. The financial support from Eni, Statoil, Lundin, Total, JFE Steel Corporation, Posco, Kobe Steel, SSAB, Bredero Shaw, Borealis, Trelleborg, Nexans, Aker Solutions, FMC Kongsberg Subsea, Kværner Verdal, Marine Aluminium, Hydro and Sapa are also acknowledged.

References

[1] A.L. Gurson, Continuum theory of ductile rupture by void nucleation and growth: Part I—yield criteria and flow rules for porous ductile media, J. Eng. Mater. Technol. 99 (1) (1977) 2–15.
[2] V. Tvergaard, A. Needleman, Analysis of the cup-cone fracture in a round tensile bar, Acta Metall. 32 (1) (1984) 157–169.
[3] Z.L. Zhang, C. Thaulow, J. Ødegård, A complete Gurson model approach for ductile fracture, Eng. Fract. Mech. 67 (2) (2000) 155–168.
[4] T. Pardoen, J.W. Hutchinson, An extended model for void growth and coalescence, J. Mech. Phys. Solids 48 (12) (2000) 2467–2512.
[5] G. Rousselier, Ductile fracture models and their potential in local approach of fracture, Nucl. Eng. Des. 105 (1) (1987) 97–111.
[6] A. Pineau, A.A. Benzerga, T. Pardoen, Failure of metals I: brittle and ductile fracture, Acta Mater. 107 (2016) 424–483.
[7] R.O. Ritchie, J.F. Knott, J.R. Rice, On the relationship between critical tensile stress and fracture toughness in mild steel, J. Mech. Phys. Solids 21 (6) (1973) 395–410.
[8] F.M. Beremin, A. Pineau, F. Mudry, J.-C. Devaux, Y. D'Escatha, P. Ledermann, A local criterion for cleavage fracture of a nuclear pressure vessel steel, Metall. Mater. Trans. 14 (11) (1983) 2277–2287.
[9] T. Lin, A.G. Evans, R.O. Ritchie, A statistical model of brittle fracture by transgranular cleavage, J. Mech. Phys. Solids 34 (5) (1986) 477–497.
[10] K. Wallin, T. Saario, K. Törrönen, Statistical model for carbide induced brittle fracture in steel, Met. Sci. 18 (1) (1984) 13–16.
[11] M.K. Samal, M. Seidenfuss, E. Roos, B.K. Dutta, H.S. Kushwaha, Experimental and numerical investigation of ductile-to-brittle transition in a pressure vessel steel, Mater. Sci. Eng. 496 (1) (2008) 25–35.
[12] M.K. Samal, J.K. Chakravartty, M. Seidenfuss, E. Roos, Evaluation of fracture toughness and its scatter in the DBTT region of different types of pressure vessel steels, Eng. Fail. Anal. 18 (1) (2011) 172–185.
[13] V. Tvergaard, A. Needleman, An analysis of the temperature and rate dependence of Charpy V-notch energies for a high nitrogen steel, Int. J. Fract. 37 (3) (1988) 197–215.
[14] V. Tvergaard, A. Needleman, An analysis of the brittle-ductile transition in dynamic crack growth, Int. J. Fract. 59 (1) (1993) 53–67.
[15] A. Needleman, V. Tvergaard, Numerical modeling of the ductile-brittle transition, Int. J. Fract. 101 (1) (2000) 73.
[16] A. Rossoll, C. Berdin, C. Prioul, Determination of the fracture toughness of a low alloy steel by the instrumented Charpy impact test, Int. J. Fract. 115 (3) (2002) 205–226.
[17] B. Tanguy, J. Besson, R. Piques, A. Pineau, Ductile to brittle transition of an A508 steel characterized by Charpy impact test: Part I: experimental results, Eng. Fract. Mech. 72 (1) (2005) 49–72.
[18] B. Tanguy, J. Besson, R. Piques, A. Pineau, Ductile to brittle transition of an A508 steel characterized by Charpy impact test: Part II: modeling of the Charpy transition curve, Eng. Fract. Mech. 72 (3) (2005) 413–434.
[19] G. Hütter, T. Linse, S. Roth, U. Mühlich, M. Kuna, A modeling approach for the complete ductile–brittle transition region: cohesive zone in combination with a nonlocal Gurson-model, Int. J. Fract. 185 (1) (2014) 129–153.
[20] A. Shterenlikht, I.C. Howard, The CAFE model of fracture—application to a TMCR steel, Fatigue Fract. Eng. Mater. Struct. 29 (9–10) (2006) 770–787.
[21] A. Shterenlikht, 3D CAFE Modelling of Transitional Ductile-Brittle Fracture in Steel, The University of Sheffield, UK, 2003.
[22] A. Shterenlikht, I.C. Howard, Cellular Automata Finite Element (CAFE) Modelling of Transitional Ductile-Brittle Fracture in Steel, the 15th European Conference of Fracture (ECF15), KTH, Stockholm, Sweden, 2004.
[23] S.J. Wu, C.L. Davis, A. Shterenlikht, I.C. Howard, Modeling the ductile-brittle transition behavior in thermomechanically controlled rolled steels, Metall. Mater. Trans. 36 (4) (2005) 989–997.
[24] S. Das, A. Shterenlikht, I.C. Howard, E.J. Palmiere, A general method for coupling microstructural response with structural performance, Proc. Math. Phys. Eng. Sci. 462 (2071) (2006) 2085–2096.
[25] A. Shterenlikht, L. Margetts, Three-dimensional cellular automata modelling of cleavage propagation across crystal boundaries in polycrystalline microstructures, Proc. Roy. Soc. Lond.: Math. Phys. Eng. Sci. 471 (2015) 2177.
[26] Standard Test Method for Determination of Reference Temperature, T0, for Ferritic Steels in the Transition Range (ASTM E1921-18), American Society for Testing and Materials, 2018.
[27] J.P. Petti, R.H. Dodds, Calibration of the Weibull stress scale parameter, σu, using the Master Curve, Eng. Fract. Mech. 72 (1) (2005) 91–120.
[28] B. Wasiluk, J.P. Petti, R.H. Dodds, Temperature dependence of Weibull stress parameters: studies using the Euro-material, Eng. Fract. Mech. 73 (8) (2006) 1046–1069.
[29] Y. Cao, H. Hui, G. Wang, F.-Z. Xuan, Inferring the temperature dependence of Beremin cleavage model parameters from the Master Curve, Nucl. Eng. Des. 241 (1) (2011) 39–45.
[30] G. Qian, V.F. González-Albuixech, M. Niffenegger, Calibration of Beremin model with the master curve, Eng. Fract. Mech. 136 (2015) 15–25.
[31] X. Gao, G. Zhang, T.S. Srivatsan, A probabilistic model for prediction of cleavage fracture in the ductile-to-brittle transition region and the effect of temperature on model parameters, Mater. Sci. Eng. 415 (1) (2006) 264–272.
[32] M. Moattari, I. Sattari-Far, I. Persechino, N. Bonora, Prediction of fracture toughness in ductile-to-brittle transition region using combined CDM and Beremin models, Mater. Sci. Eng. 657 (2016) 161–172.
[33] Y. Li, X. Ren, J. He, Z. Zhang, Constraint effect on the brittle-to-ductile transition of single-crystal iron induced by dislocation mobility, Int. J. Mech. Sci. 149 (2018) 212–223.
[34] M. Stec, J. Faleskog, Micromechanical modeling of grain boundary resistance to cleavage crack propagation in ferritic steels, Int. J. Fract. 160 (2) (2009) 151.
[35] V.R. Nitzsche, K.J. Hsia, Modelling of dislocation mobility controlled brittle-to-ductile transition, Mater. Sci. Eng. 176 (1) (1994) 155–164.
[36] A. Hartmaier, P. Gumbsch, Thermal activation of crack-tip plasticity: the brittle or ductile response of a stationary crack loaded to failure, Phys. Rev. B 71 (2) (2005) 024108.
[37] A.S. Argon, Mechanics and physics of brittle to ductile transitions in fracture, J. Eng. Mater. Technol. 123 (1) (2000) 1–11.
[38] ASTM E23-18 Standard Test Methods for Notched Bar Impact Testing of Metallic Materials, (2018).
[39] A. Giannattasio, M. Tanaka, T.D. Joseph, S.G. Roberts, An empirical correlation between temperature and activation energy for brittle-to-ductile transitions in single-phase materials, Phys. Scripta (2007) 87 (T128) (2007).
[40] M. Tanaka, K. Higashida, T. Shimokawa, T. Morikawa, Brittle-ductile transition in low carbon steel deformed by the accumulative roll bonding process, Mater. Trans. 50 (1) (2009) 56–63.
[41] P.B. Hirsch, S.G. Roberts, The brittle-ductile transition in silicon, Philos. Mag. A 64 (1) (1991) 55–80.
[42] G.W. Hollenberg, G.R. Terwilliger, R.S. Gordon, Calculation of stresses and strains in four-point bending creep tests, J. Am. Ceram. Soc. 54 (4) (1971) 196–199.
[43] T. Fett, Stress Intensity Factors – T-Stresses – Weight Functions, Supplement Volume, KIT Scientific Publishing, 2009.
[44] P. Bowen, S.G. Druce, J.F. Knott, Effects of microstructure on cleavage fracture in pressure vessel steel, Acta Metall. 34 (6) (1986) 1121–1131.
[45] M. Kroon, J. Faleskog, Micromechanics of cleavage fracture initiation in ferritic steels by carbide cracking, J. Mech. Phys. Solids 53 (1) (2005) 171–196.
[46] T. Lin, A.G. Evans, R.O. Ritchie, Stochastic modeling of the independent roles of particle size and grain size in transgranular cleavage fracture, Metall. Mater. Trans. 18 (4) (1987) 641–651.
[47] J.I. San Martin, J.M. Rodriguez-Ibabe, Determination of energetic parameters controlling cleavage fracture in a Ti-V microalloyed ferrite-pearlite steel, Scripta Mater. 40 (4) (1999) 459–464.
[48] L. Rancel, M. Gómez, S.F. Medina, I. Gutierrez, Measurement of bainite packet size and its influence on cleavage fracture in a medium carbon bainitic steel, Mater. Sci. Eng. 530 (2011) 21–27.
[49] A. Ghosh, A. Ray, D. Chakrabarti, C.L. Davis, Cleavage initiation in steel: competition between large grains and large particles, Mater. Sci. Eng. 561 (2013) 126–135.
[50] M.A. Linaza, J.M. Rodriguez-Ibabe, J.J. Urcola, Determination of the energetic parameters controlling cleavage fracture initiation in steels, Fatigue Fract. Eng. Mater. Struct. 20 (5) (1997) 619–632.
[51] S. Lee, S. Kim, B. Hwang, B.S. Lee, C.G. Lee, Effect of carbide distribution on the fracture toughness in the transition temperature region of an SA 508 steel, Acta Mater. 50 (19) (2002) 4755–4762.
[52] S. Kim, S. Lee, B.S. Lee, Effects of grain size on fracture toughness in transition temperature region of Mn–Mo–Ni low-alloy steels, Mater. Sci. Eng. 359 (1) (2003) 198–209.
[53] H.W. Schadler, Mobility of edge dislocations on {110} planes in tungsten single crystals, Acta Metall. 12 (8) (1964) 861–870.
[54] H.A. Khater, D.J. Bacon, Dislocation core structure and dynamics in two atomic models of α-zirconium, Acta Mater. 58 (8) (2010) 2978–2987.